MHD Simulations of Pellet Injection in the LHD*)

Ryuichi ISHIZAKI and Noriyoshi NAKAJIMA
National Institute for Fusion Science, Toki 509-5292, Japan
(Received 11 December 2013 / Accepted 21 April 2014)

To clarify motions of a plasmoid induced by pellet ablation in the Large Helical Device (LHD), MHD simulations have been conducted. When a plasmoid is located on the inboard side of the mid-plane in the LHD, it drifts in the negative direction of the major radius not only on the horizontally elongated poloidal cross section but also on the vertically elongated poloidal cross section. This means that the plasmoid drifts to the lower field side in the former and to the higher field side in the latter. Our simulations show that these motions are determined by the direction of the curvature vector and the magnetic pressure distribution along the field line at the location of the plasmoid.

Keywords: pellet, ablation, MHD, CIP, LHD

DOI: 10.1585/pfr.9.3403130

1. Introduction

Injecting small pellets of frozen hydrogen into torus plasmas is a proven method of fueling [1]. Since a high-density low-temperature plasmoid induced by pellet ablation drifts to the low-field side, pellet fueling to make the plasmoid approach the core plasma in a tokamak is successful when a pellet is injected from the high-field side. However, such good performance has not yet been obtained in experiments in the planar axis heliotron, the Large Helical Device (LHD), even when a pellet was injected from the high-field side [2]. To clarify the difference in plasmoid motions in a tokamak and in the LHD, a three-dimensional (3D) magnetohydrodynamics (MHD) code including ablation processes has been developed by extending the pellet ablation code (CAP) [3, 4]. In the LHD, drift motion depends on the initial location of the plasmoid, whereas in a tokamak, the plasmoid always drifts in the direction of the major radius [5]. Especially, when the plasmoid is located on the inboard side of the mid-plane in the LHD, the plasmoid drifts in the negative direction of the major radius not only on the horizontally elongated poloidal cross section but also on the vertically elongated poloidal cross section. This means that plasmoids drift to the lower field side in the former and to the higher field side in the latter. In this paper, we report simulation results that explain the physical mechanisms causing this behavior.

2. Plasmoid Motion in the LHD

Since linear theory cannot be applied to a plasmoid because of its large perturbations, nonlinear simulations are required to explain plasmoid behavior. Plasmoid drift is considered to be an MHD phenomenon because the drift speed obtained from experiments [1] is several percent of the Alfvén velocity. Thus, a 3D MHD code including ablation processes has been developed by extending the CAP code. To investigate plasmoid motion in the LHD plasmas, an equilibrium state obtained from the HINT code [6] is used as the bulk plasma. The cubic-interpolated pseudoparticle (CIP) method is used in the code as the numerical scheme [7], and cylindrical coordinate (R, φ, Z) is used. All physical variables are normalized by a length of 1 m, time of 10^{-6} s, magnetic field of 0.62 T, and hydrogen number density of $0.8 \times 10^{20}\,\mathrm{m}^{-3}$.

Figure 1 (a) shows the plasma beta and rotational transform of the LHD used in the simulations. The maximum and average beta are 3.6% and 1.0%, respectively, and the magnetic axis is located at $R = 3.8$ m. As shown in Fig. 1 (b), plasmoid 1 is located on the inboard side of the mid-plane on the horizontally elongated poloidal cross section. As an initial condition, it is assumed that the peak value of the plasmoid density is 1000 times the density of the bulk plasma. It is also assumed that the plasmoid has no perturbations in the pressure and magnetic field so that an initial force balance is satisfied and there are no artificial conditions. The plasmoid, whose half-width is 0.03, encounters electrons with a fixed temperature of 1 keV and density of $0.8 \times 10^{20}\mathrm{m}^{-3}$. The helical plasma has a saddle point in the magnetic pressure near the core on the poloidal cross section. Figure 1 (c) shows the magnetic pressure and the R-component of the curvature vector as functions of R on the mid-plane. The saddle point is located at $R = 3.75$, where the magnetic pressure is a maximum in the R-direction and a minimum in the Z-direction. In addition, the curvature vector is almost zero. Then, plasmoid 1 is located in a lower-field than the saddle point. Figure 2 shows the temporal evolution of the average plasmoid 1 density on the flux surface with the Boozer coor-

author's e-mail: ishizaki@nifs.ac.jp
*) This article is based on the presentation at the 23rd International Toki Conference (ITC23).

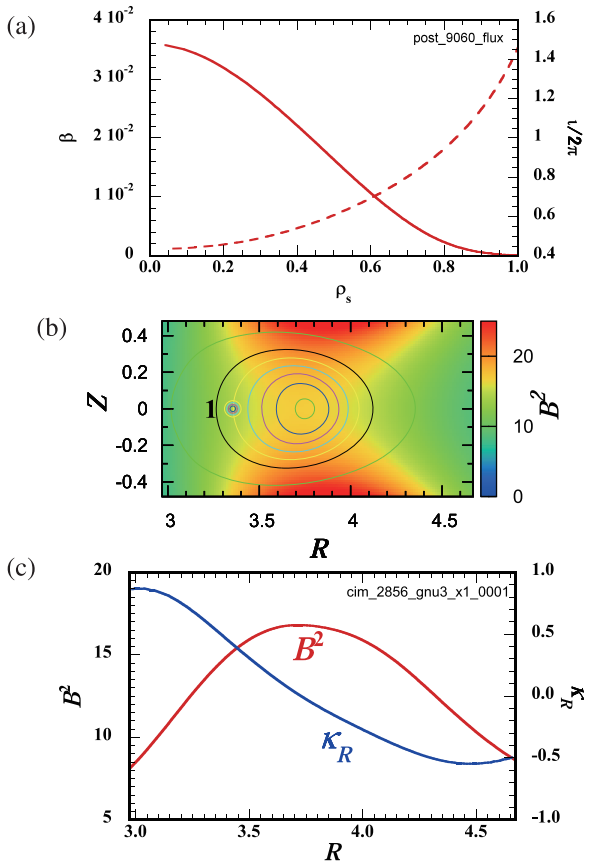

Fig. 1 (a) Plasma beta β (solid line) and rotational transform $\iota/2\pi$ (dashed line) as functions of normalized minor radius ρ_s. (b) Horizontally elongated poloidal cross section in the LHD. Colors and contours show the equilibrium magnetic and plasma pressures, respectively. Circle shows the initial position of plasmoid 1. (c) Magnetic pressure (red) and R-component of the curvature vector (blue) as functions of R at $Z = 0$ on the horizontally elongated poloidal cross section.

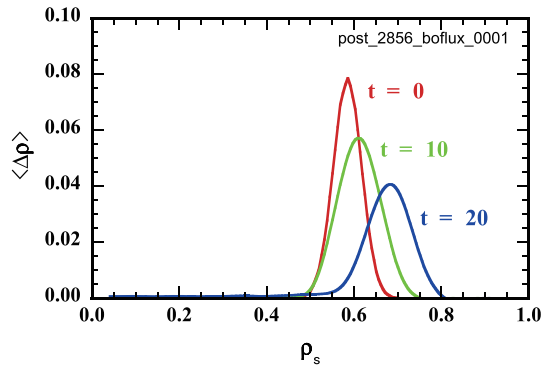

Fig. 2 Temporal evolution of the average density of plasmoid 1 on the flux surface as a function of ρ_s with the Boozer coordinate.

dinate. The plasmoid drifts in the direction of the minor radius. This means that the plasmoid drifts to the lower field side and in the direction opposite to that of the curvature vector because the plasmoid is located on the left-hand side of the core center, as shown in Fig. 1 (b). The maximum value of the density decreases with time, as shown in Fig. 2. This is because the plasmoid is not only elongated along the field line but also expanded across the flux surface, and the area of each flux surface is different.

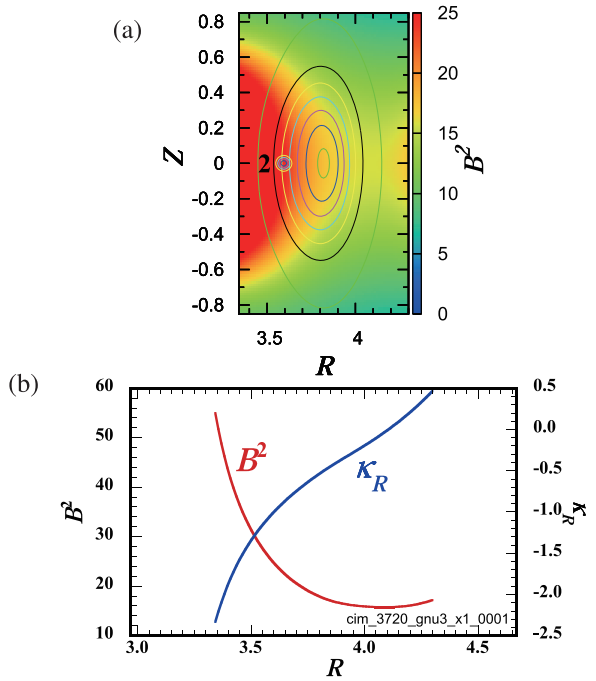

Fig. 3 (a) Vertically elongated poloidal cross section in the LHD. Colors and contours show the equilibrium magnetic and plasma pressures, respectively. Circle shows the initial location of plasmoid 2. (b) Magnetic pressure (red) and R-component of the curvature vector (blue) as functions of R at $Z = 0$ on the vertically elongated poloidal cross section.

Plasmoid 2 is located on the inboard side of the mid-plane in the vertically elongated poloidal cross section, as shown in Fig. 3 (a). Figure 3 (b) shows the magnetic pressure and R-component of the curvature vector as functions of R on the mid-plane. A saddle point is located at $R = 4.1$, where the magnetic pressure is a minimum in the R-direction and a maximum in the Z-direction, and the curvature vector is almost zero. Then, plasmoid 2 is located in a higher field than the saddle point. Figure 4 shows the temporal evolution of the average plasmoid 2 density on the flux surface with the Boozer coordinate. In the initial phase, the plasmoid drifts in the negative direction of the minor radius, then subsequently it drifts in the positive direction. In other words, the plasmoid drifts first to the lower field side, and then to the higher field side. This motion is clearly different from that of plasmoid 1. The physical mechanisms behind these differences in behavior are discussed in section 3.

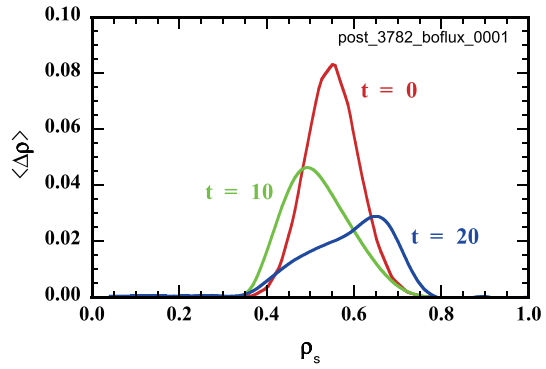

Fig. 4 Temporal evolution of the average density of plasmoid 2 on the flux surface as a function of ρ_s with the Boozer coordinate.

3. Discussion

The force acting on a plasmoid located on the mid-plane is approximately given by $\boldsymbol{B}^{eq} \cdot \nabla \boldsymbol{B}^{pl}$, where $\boldsymbol{B}^{eq}$ is the equilibrium magnetic field and $\boldsymbol{B}^{pl}$ is a perturbation of the magnetic field [5]. Then, the R-component of the force is expressed as follows.

$$F_R = \boldsymbol{e}_R \cdot \left(\boldsymbol{B}^{eq} \cdot \nabla \boldsymbol{B}^{pl} \right) = \boldsymbol{B}^{eq} \cdot \nabla B_R^{pl} - \frac{B_\varphi^{eq} B_\varphi^{pl}}{R}. \quad (1)$$

The first term in Eq. (1) represents the gradient of B_R^{pl} along the equilibrium magnetic field, and the second term represents the $1/R$ force due to the toroidal field [8]. Figures 5 (a) and 5 (b) show the temporal evolutions of accelerations of plasmoids 1 and 2, respectively. The red, green, and blue lines show the first term, second term and total force F_R in Eq. (1), respectively. The second term in Eq. (1) is always positive because the sign of B_φ^{pl} differs from that of B_φ^{eq} due to the diamagnetic effect. In contrast, the sign of the first term is determined by the structure of the magnetic field. In other words, when the plasmoid drifts in the negative R direction, the first term should be negative and its absolute value should be greater than that of the second term. This is shown in Figs. 5 (a) and 5 (b). The second term is dominant in a tokamak, and the first term is dominant in the LHD when the plasmoid is located on the inboard side of the mid-plane [5].

To clarify the physical mechanism for the behavior of plasmoid 1, the first and second terms in Eq. (1) have been evaluated. Figure 6 shows the first and second terms as functions of R through the center of plasmoid 1 at (a) $t = 1$ and (b) $t = 18.2$. As mentioned above, the second term is always positive within the plasmoid. The behaviors of the first terms in Figs. 6 (a) and 6 (b) can be explained by using the diagrams in Figs. 7 (a) and 7 (b), respectively. The latter figures show the plasmoid and magnetic field on the R-φ plane at $z = 0$, i.e., on the mid-plane. In the initial phase, plasmoid 1 is not only elongated along the magnetic field line but also expanded perpendicular to it, as shown in

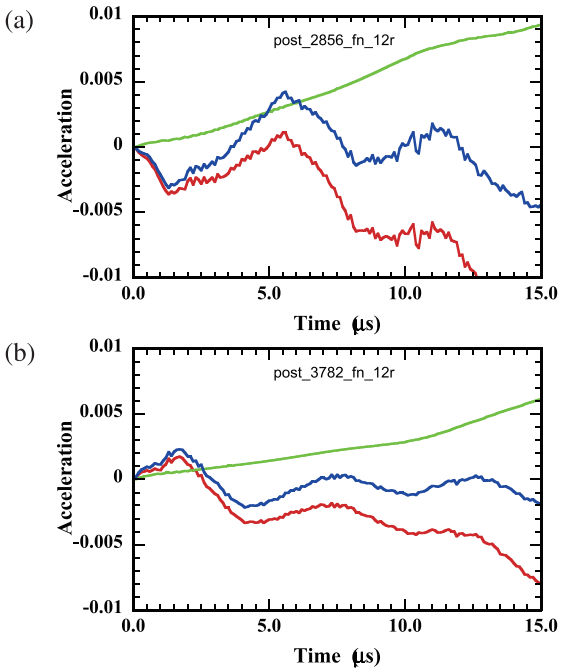

Fig. 5 Acceleration as a function of time for (a) plasmoid 1 and (b) plasmoid 2. Red, green, and blue lines show the acceleration due to the first term, second term, and total force, respectively, in Eq. (1).

Fig. 7 (a). Because of such plasmoid motion, the magnetic field lines a and b (black curves) change to a' and b' (red curves), respectively. The R-component of the magnetic field perturbation, B_R^{pl}, is induced by the plasmoid motion, as shown by the green arrows. Since the magnetic curvature of field line a is greater than that of field line b, the change from a to a' is also greater than that from b to b'. Then, the first term, $\boldsymbol{B}^{eq} \cdot \nabla B_R^{pl}$, becomes negative at field line a and positive at field line b. The absolute value for field line a is greater than that for field line b. This corresponds to the force in Fig. 6 (a). As a result, the force acting on the plasmoid by the first term becomes negative, as shown by the blue arrow in Fig. 7 (a). After the initial phase, the plasmoid shape forms an ellipse due to elongation along the field line, as shown in Fig. 7 (b). In that figure, plasmoid 1 is on the left because it is located on the inboard side of the mid-plane. The equilibrium magnetic pressure along the field line is a local minimum at $\varphi = 0$. This means that the plasmoid is elongated to the higher field side along the field line. Since the flow of the plasmoid along the field line is inhibited by the magnetic pressure, the flow becomes narrow, as shown in Fig. 7 (b). Due to such plasmoid flow, the magnetic field lines a and b (black curves) change to a' and b' (red curves), respectively. The R-component of the magnetic field perturbation, B_R^{pl}, is induced, as shown by the green arrows. Since the magnetic curvature of field line a is greater than that of field line b, the change from a to a' is also greater than that from b to b'. Then, the first term, $\boldsymbol{B}^{eq} \cdot \nabla B_R^{pl}$, becomes negative at field line a and positive at field line b. The absolute

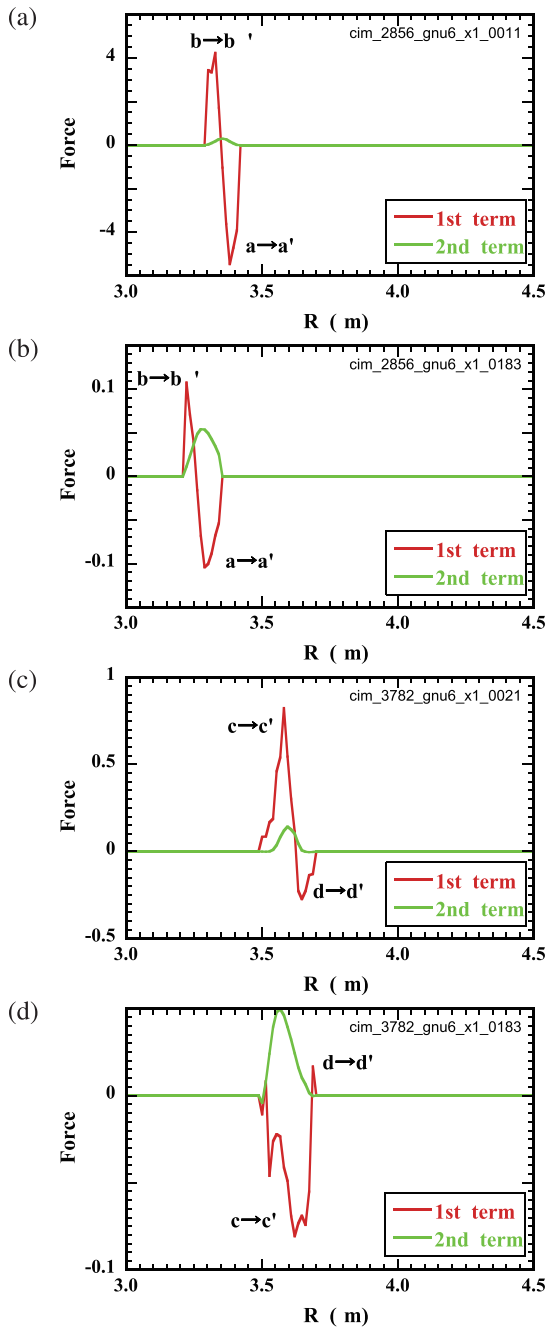

Fig. 6 First term (red line) and second term (green line) in Eq. (1) as functions of R through the center of the plasmoid. Those for plasmoid 1 are at (a) $t = 1$ and (b) $t = 18.2$. Those for plasmoid 2 are at (a) $t = 2$ and (b) $t = 18.2$.

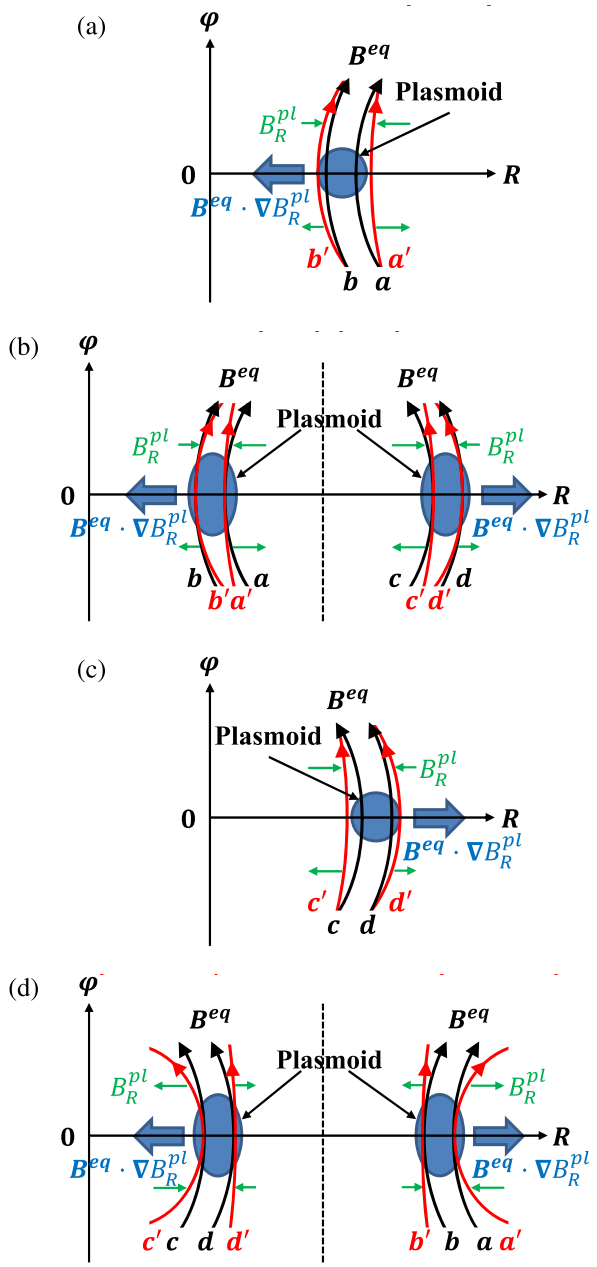

Fig. 7 Diagrams explaining the physical mechanism causing the behavior of $\boldsymbol{B}^{eq} \cdot \nabla B_R^{pl}$ on the R-φ plane at $z = 0$. Motions of plasmoid 1 (a) during and (b) after the initial phase. Motions of plasmoid 2 (c) during and (d) after the initial phase. Plasmoids are denoted by blue circles and ellipses. Magnetic field lines a, b, c, and d (black curves) change to a', b', c', and d' (red curves), respectively, due to plasmoid motion. B_R^{pl} is denoted by green arrows. The forces, $\boldsymbol{B}^{eq} \cdot \nabla B_R^{pl}$, are denoted by blue arrows. Vertically dashed lines show the magnetic axes.

value of field line a is greater than that of field line b. This corresponds to the force in Fig. 6 (b). As a result, the force acting on the plasmoid by the first term becomes negative, as shown by the blue arrow in Fig. 7 (b), and the plasmoid drifts to the lower field side. These interpretations explain the plasmoid behaviors in Figs. 2 and 5 (a). The oscillations with a period of about 5 μs, shown in Fig. 5, is induced by the restoring force of the magnetic field.

The physical mechanism for the behavior of plasmoid 2 can be explained by using Figs. 6 (c), 6 (d), 7 (c), and 7 (d). Figure 6 shows the first and second terms in Eq. (1) as functions of R through the center of plasmoid 2 at (c) $t = 2$ and (d) $t = 18.2$. The second term is always positive within the plasmoid, as mentioned above. In the initial phase, the plasmoid is not only elongated along the

magnetic field line but also expanded perpendicular to it, as shown in Fig. 7 (c). The R-component of the magnetic field perturbation, B_R^{pl}, is induced by the plasmoid motion, as shown by the green arrows. The first term, $\boldsymbol{B}^{eq} \cdot \nabla B_R^{pl}$, becomes positive at field line c and negative at field line d. This corresponds to the force in Fig. 6 (c). Then, the force acting on the plasmoid by the first term becomes positive, as shown by the blue arrow. After the initial phase, the plasmoid shape forms an ellipse due to elongation along the field line, as shown in Fig. 7 (d) in which plasmoid 2 is on the left because it is located on the inboard side of the mid-plane. The equilibrium magnetic pressure along the field line is a local maximum at $\varphi = 0$. Since the plasmoid is elongated to the lower field side along the field line, the flow of the plasmoid along the field line becomes broad, as shown in Fig. 7 (d). Due to such plasmoid flow, the magnetic field lines c and d (black curves) change to c' and d' (red curves), respectively. In other words, the R-component of the magnetic field perturbation, B_R^{pl}, is induced, as shown by the green arrows. Since the magnetic curvature of field line c is greater than that of field line d, the change from c to c' is also greater than that from d to d'. Then, the first term, $\boldsymbol{B}^{eq} \cdot \nabla B_R^{pl}$, becomes negative at field line c and positive at field line d. The absolute value of field line c is greater than that of field line d. This corresponds to the force in Fig. 6 (d). As a result, the force acting on the plasmoid by the first term becomes negative, as shown by the blue arrow in Fig. 7 (d), and the plasmoid drifts to the higher field side. These interpretations explain the behaviors in Figs. 4 and 5 (b).

Since plasmoids 1 and 2 are located on the inboard side of the mid-plane on the horizontally and vertically elongated poloidal cross sections, respectively, the R-components of the curvature vectors for the plasmoids are positive and negative, respectively. However, the magnetic pressures along the field lines for plasmoids 1 and 2 are a local minimum and maximum, respectively. We find that these structures of the magnetic fields are essential to explain the plasmoid motions in terms of the physical mechanisms shown in Fig. 7.

4. Summary

Although a plasmoid induced by pellet ablation drifts to the lower field side in a tokamak, plasmoid motion depends on the structure of the magnetic field in the LHD. In particular, a plasmoid located on the inboard side of the mid-plane drifts to the higher field side on the vertically elongated poloidal cross section. We have shown that this motion is determined by the direction of the curvature vector and the magnetic pressure distribution along the field line at the location of the plasmoid.

[1] Y.W. Muller *et al.*, Nucl. Fusion **42**, 301 (2002).
[2] R. Sakamoto *et al.*, Nucl. Fusion **44**, 624 (2004).
[3] R. Ishizaki *et al.*, Phys. Plasmas **11**, 4064 (2004).
[4] R. Ishizaki *et al.*, IAEA-CN-149/TH/P3-6 (2006).
[5] R. Ishizaki and N. Nakajima, Plasma Phys. Control. Fusion **53**, 054009 (2011).
[6] K. Harafuji *et al.*, J. Comput. Phys. **81**, 169 (1989).
[7] H. Takewaki *et al.*, J. Comput. Phys. **61**, 261 (1985).
[8] J.P. Freidberg, *Ideal Magnetohydrodynamics* (New York: Plenum, 1987).